Ring-shaped luminescence pattern in biased quantum wells studied as a steady-state reaction front

Masudul Haque
Institute for Theoretical Physics, Utrecht University, Leuvenlaan 4, 3584 CE Utrecht, the Netherlands
(Received 9 July 2005; published 7 June 2006)

Under certain conditions, focused laser excitation in semiconductor quantum well structures can lead to a charge separation and a circular reaction front, which is visible as a ring-shaped photoluminescence pattern. The diffusion-reaction equations governing the system are studied here with the aim of a detailed understanding of the steady state. The qualitative asymmetry in the sources for the two carriers is found to lead to unusual effects which dramatically affect the steady-state configuration. Analytic expressions are derived for carrier distributions and interface positions for a number of cases. These are compared with steady-state information obtained from simulations of the diffusion-reaction equations.

DOI: 10.1103/PhysRevE.73.066207 PACS number(s): 89.75.Kd, 78.67.De, 66.30.Pa, 71.35.Lk

I. INTRODUCTION

In mid 2002, two semiconductor-optics experimental groups reported dramatic ring-shaped photoluminescence patterns when a focused laser was used to excite electron-hole pairs near a coupled quantum well system biased with an electric field [1,2]. Despite initial speculation invoking Bose-Einstein condensation of excitons, it was later found that the luminescence ring is well explained by classical reaction-diffusion dynamics of the electrons and holes [3,4]. The idea is that there is a net hole injection into the quantum well near the laser irradiation spot, together with an electron source due to a leakage current that is roughly uniform across the two-dimensional (2D) quantum well plane. This combination can lead to a charge-separated steady-state configuration, with a circular hole-rich island sustained by the localized hole source in an electron-rich sea. The interface, where outward-diffusing holes recombine with inward-diffusing electrons, is the luminescence ring.

The position of the interface, i.e., the radius of the luminescence ring, is not well understood theoretically, despite some theoretical [3,5] and experimental [5,6] efforts. While a full understanding may or may not require extra ingredients in addition to the diffusion-reaction model [5], a thorough study of the behavior of the interface position *within* the diffusion model is certainly a necessary first step. The present paper fills this gap by presenting a detailed analysis of the steady state, addressing aspects such as the position and width of the interface, density distributions, etc. There are a number of length scales in the problem which we identify cleanly. The phenomenon is put into the context of previous theoretical studies of steady-state reaction fronts and variations thereof [7–15]. By considering various possible relative values of the tunneling decay rates of the two carrier species, we clarify the roles of the tunneling strengths in determining the steady-state configuration. A curious feature of the steady state is that the reaction zone has, in addition to the sharp interface, an extended feature on one side where the luminescence does not vanish but instead is a nonzero constant. This aspect turns out to have a drastic influence on the interface position and the overall steady-state structure, which we explain in detail.

In comparison with previous theoretically studied diffusion-annihilation systems [7–15], the present problem has several unusual features which justify an extended study. These include the single-particle (tunneling) decay of one or both species, and the fact that one of the reacting species has a spatially extended source spanning both sides of the interface. In addition, while diffusion-controlled reaction interfaces and patterns have been studied in a wide variety of chemical, biological, and fluid flow contexts [16–18], they are rather rare in electronic systems. Indeed, this may well be the only currently known example of a diffusion-limited nonequilibrium reaction front or pattern in electronic systems. Furthermore, there is the intriguing possibility of studying quantum phenomena in the ring region [19,20], where the carriers have had time to cool down to quantum degeneracy.

Section II introduces the diffusion-reaction equations, simplifying source details, and also presents the important length scales. Section III contains the analysis of the steady state and the main results of this paper. In Sec. IV, our calculations are put into perspective by discussing experimental issues and briefly reviewing the relevant theoretical literature. The method used for numerical evolution of the diffusion-reaction equations is outlined in Appendix A.

II. DIFFUSION-REACTION MODEL

For experimental details beyond what is sketched here, the reader is referred to Refs. [1,2,6,22]. The phenomenon occurs in a two-dimensional quantum well system, either a single well or two closely separated parallel wells. Electron-hole pairs are created in the vicinity of the well(s), mainly in the substrate, by a focused laser excitation.

A voltage is applied across the well(s) using conducting electron-rich (n^+) regions on both sides of the well(s) as leads. The original motivation was to enhance the lifetime of excitons or electron-hole gases by spatially separating electrons and holes in the direction transverse to the well(s). A band-structure cartoon of the experimental setup is shown in the inset of Fig. 1. Due to the electric field bias, there is an influx current of electrons into the well as well as a tunneling-out process. In addition, the holes can tunnel out in the other direction; this corresponds to an electron from the

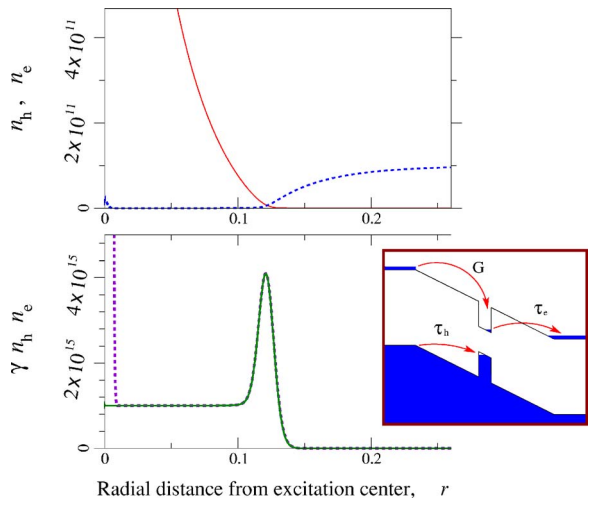

FIG. 1. (Color online) Top panel: steady-state carrier density distributions. n_h dominates at small r and n_e dominates at large r. Bottom panel: luminescence profile. Dashed and solid lines correspond to $P_e \neq 0$ and $P_e = 0$, respectively. The hole excess $P_h - P_e$ is the same in the two cases, so that the only difference is in the structure around $r=0$. Lower-right inset: band-structure schematic (single well). Arrows indicate tunneling processes described in text.

left lead or substrate filling up one of the hole states in the well. The three processes are shown by arrows in the Fig. 1 inset. Note that there is no source of holes due to the biasing. Holes are only created by photoexcitation.

Incorporating the above effects, one can write down two-dimensional diffusion-annihilation equations for the densities of holes (n_h) and electrons (n_e) within the quantum well(s):

$$\frac{\partial n_h}{\partial t} = D_h \nabla^2 n_h + P_h e^{-r^2/l_L^2} - \gamma n_h n_e - \frac{1}{\tau_h} n_h, \tag{1a}$$

$$\frac{\partial n_e}{\partial t} = D_e \nabla^2 n_e + P_e e^{-r^2/l_L^2} - \gamma n_h n_e + G - \frac{1}{\tau_e} n_e. \tag{1b}$$

The $D_{h,e}$ are diffusion constants. The $n_{h,e}/\tau_{h,e}$ terms model decay due to carriers tunneling out of the well(s), the τ's being tunneling lifetimes. G is the spatially uniform source term for electrons, which is absent for holes. The γ terms represent electron-hole recombination. The $P_{h,e}$ terms are the laser excitation terms; the laser is focused onto a spot roughly of radius l_L.

By numerically evolving Eqs. (1) in time, one can determine the steady-state carrier distributions and luminescence after $P_{h,e}$ are turned on. A typical steady-state distribution, obtained with $P_h > P_e$, is shown in Fig. 1. The simulation (Appendix A) is one-dimensional, so that radial plots are sufficient. The steady state displays a species-separated configuration, together with a peak in the luminescence marking the interface, as described previously. For $P_e \neq 0$, the luminescence profile also shows an inner peak near $r=0$, corresponding roughly to a central luminescence spot observed experimentally.

Typical values of the parameters are taken to be of the following orders: D's, several cm^2/s; τ's, 10^{-4} s; γ, 10^{-3} s^{-1} cm^2; l_L, 10^{-3} cms; G, 10^{15} s^{-1} cm^{-2}; and Pl_L^2's, 10^{12} s^{-1}. Units will be omitted in the rest of this paper.

Equation (1), with several variations, was proposed in Refs. [3,4] as the luminescence ring mechanism, and studied further in Refs. [5,6,19–21]. For a restricted case, Ref. [3] also contains a minimal analytic treatment of the steady state.

For the charge separation phenomenon, we need more holes diffusing out of the excitation region than electrons. In previous studies [3–6], the philosophy has been to invoke differences of unknown origin in the efficiency of accumulation in the well(s), i.e., to use $P_h > P_e$ without detailed explanation. The current understanding of the carrier asymmetry is thus unsatisfactory. In fact, it is possible to have an excess of holes and a resulting luminescence ring with $P_h = P_e$. However, the present author will postpone to a future publication an analysis of the source asymmetry and of the inner spot structure.

Since we neglect the inner structure in this study, it is convenient to drop the electron source altogether ($P_e=0$), and assume a point source for the holes, i.e., $P_h e^{-r^2/l_L^2}$ is replaced by $P_x \delta(\mathbf{r})$. For comparison with the numeric simulations, where a finite l_L has been used, the correspondence is $P_x \equiv \pi l_L^2 P_h$. This is obtained by equating an outward flux for the point and Gaussian sources. One result of omitting the electron source is the absence of an inner luminescence spot (Fig. 1, solid line in lower panel). Moreover, the expressions for hole density in Sec. III will diverge at the illumination spot. This (minor) unphysical result is a result of the unphysical "point" source.

We now identify the length scales present in the problem. The two most important ones are the *depletion lengths* for electrons and holes, $l_e = \sqrt{D_e \tau_e}$ and $l_h = \sqrt{D_h \tau_h}$. The depletion lengths provide the length scales for the variation of steady-state densities, analogous to the diffusion lengths $\sqrt{Dt}$ in the literature on time-dependent front formation between two initially separated reactants [8–11], where $\sqrt{Dt}$ gives the spatial variation length scale after time t.

The ratio of the source strengths, P_x and G, provides a third length scale, which we define as $l_{src} = \sqrt{P_x/\pi G}$. The radius of the ring-shaped interface increases monotonically with the length l_{src}. The interface radius l_R itself, and the interface width l_w, are not input parameters in the problem but emerge from the analysis as important length scales. We are interested in cases where the interface is sharp, i.e., $l_w \ll l_R$.

Other lengths appearing in the problem can be expressed in terms of the ones introduced above.

III. ANALYSIS OF STEADY STATE

Analytic treatment of the steady state is simpler if one neglects the hole tunneling ($\tau_h \to \infty$), so that the hole depletion length $l_h = \sqrt{D_h \tau_h}$ disappears from the problem. Note that a finite τ_e is necessary to provide the uniform electron background at large r. It is also convenient to first consider an infinitely sharp interface ($l_w = 0$). In addition, the treatment in

Ref. [3] neglects the electron density on the hole side of the interface, and vice versa. We will consider this simplified model in III A, first without assuming anything about l_R/l_e, and then writing out both $l_R \ll l_e$ and $l_R \gg l_e$ limits.

In Sec. III B, corrections due to nonzero n_e in the hole side are derived. In Sec. III C, a finite τ_h is reinserted, and in Sec. III D the width of the sharp interface itself is studied.

A. Simplified model

With $\tau_h \to \infty$, the equations for steady state are

$$D_h \nabla^2 n_h + P_x \delta(\mathbf{r}) - \gamma n_h n_e = 0, \tag{2a}$$

$$D_e \nabla^2 n_e - \gamma n_h n_e + G - \frac{1}{\tau_e} n_e = 0. \tag{2b}$$

If the hole and electron densities are strictly zero outside and inside the ring, respectively, then the nonlinear reaction terms in Eqs. (2) then drop out both inside and outside the ring. The resulting linear equations can be exactly solved:

$$n_h(\mathbf{r}) = \frac{P_x}{2\pi D_h} \ln\left(\frac{l_R}{r}\right) \theta(l_R - r), \tag{3}$$

$$n_e(\mathbf{r}) = G\tau_e \left[1 - \frac{K_0(r/l_e)}{K_0(l_R/l_e)}\right] \theta(r - l_R). \tag{4}$$

Here $K_\nu(x)$ is a modified Bessel function of the second kind.

Note that Eq. (3) is very similar to Eq. (17) of Ref. [7], where also a steady state is analyzed. On the other hand, Eq. (4) involves a length scale (l_e), which is not so common in previous studies of steady-state fronts. Instead, it resembles more the time-dependent case of Refs. [8–11], where the corresponding length scale is determined by the time t, analogously to our τ_e.

In the $l_R \ll l_e$ limit, Eq. (4) can be written approximately as

$$n_e(\mathbf{r}) = G\tau_e \left[1 - \frac{\ln(r/l_e)}{\ln(l_R/l_e)} \theta(l_e - r)\right] \theta(r - l_R), \tag{5}$$

provided we are not interested in the $n_e(r)$ behavior for $r \gtrsim l_e$. In the limit $l_R \gg l_e$:

$$n_e(\mathbf{r}) = G\tau_e \left[1 - \frac{e^{-r/l_e}/\sqrt{r}}{e^{-l_R/l_e}/\sqrt{l_R}}\right] \theta(r - l_R). \tag{6}$$

With the expressions for the densities, one can now match the electron influx and hole outflux currents ($j = -D\nabla n$) to determine the ring radius l_R in the simplified model:

$$D_h \left[\frac{P_x}{2\pi D_h} \frac{1}{l_R}\right] = D_e \left[\frac{G\tau_e}{l_e} \frac{K_1(l_R/l_e)}{K_0(l_R/l_e)}\right]. \tag{7}$$

This equation can be solved numerically to give the ring position l_R as a function of the hole source strength P_x, or more "universally," to express l_R/l_e as a function of $(l_{src}/l_e)^2$.

The hole diffusion constant D_h drops out, and so the interface position is independent of D_h. In addition, the recombination rate γ does not enter because of the zero-width approximation for the interface. This approximation turns out to be surprisingly good as far as l_R is concerned; as long as there is a well-defined peak in the luminescence, changing γ affects the width and height of the peak profile but not the position [Fig. 2(a)]. We also note that the two source parameters enter only as the ratio P_x/G and not individually.

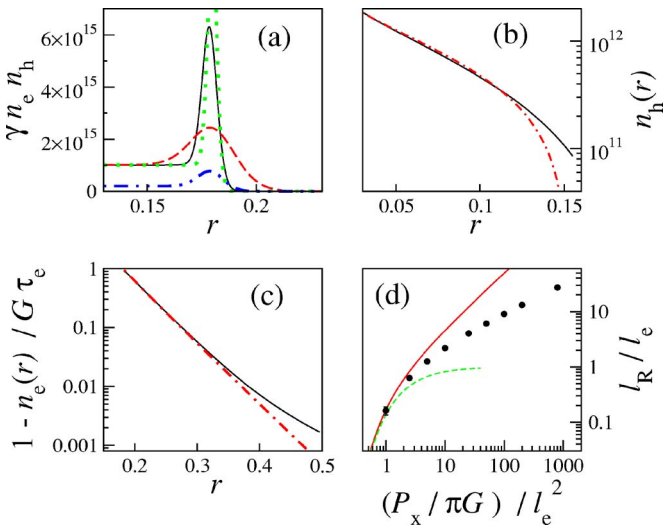

FIG. 2. (Color online) Assessment of the simple model in Sec. III A and in Ref. [3]. (a) Luminescence profiles ($\gamma n_h n_e$) shown for situations in which l_{src}, l_e are fixed but other parameters vary. Compared to the solid curve, the dashed curve has γ decreased by a factor of 25, while the dotted curve has D_h decreased by a factor of 5, all other parameters remaining fixed. Dash-dotted curve has G and P_x decreased by a factor of 5, while keeping the ratio P_x/G fixed. (b) The solid line is hole density $n_h(r < l_R)$ in a hole-rich side of the interface, from simulation. Dash-dotted line shows the best fit of the form $\sim \ln(l_R/r)$. (c) Electron density distribution $n_e(r > l_R)$ from simulation, normalized to and subtracted from $n_e(\infty) = G\tau_e$. Dash-dotted line is a fit to $K_0(r/l_e)$, Eq. (4). (d) Radius of the ring, in units of the electron depletion length l_e, plotted as a function of the hole source strength P_x, in units of $\pi G l_e^2$.

In the $l_R \ll l_e$ and $l_R \gg l_e$ limits, Eq. (7) can be solved analytically for l_R, giving, respectively,

$$l_R = l_e \exp[-2\pi G l_e^2 / P_x] = l_e \exp\left[\frac{-2}{(l_{src}/l_e)^2}\right] \tag{8}$$

and

$$l_R = P_x / 2\pi G l_e = l_{src}^2 / 2 l_e. \tag{9}$$

Equations (3), (5), and (8) have been obtained previously [3]. Ref. [3] has a spurious D_h^{-1} factor in the exponent of expression (8) for l_R.

The theory developed in this section, based on the approach of Ref. [3], is now evaluated by comparing with data from the numeric simulation (Appendix A) of the diffusion-reaction equations. In Fig. 2(a), luminescence profiles have been plotted for several cases to show that the ring radius remains unchanged if the recombination rate γ is changed (an assumption of the theory), if the hole diffusion constant D_h is changed (a prediction of the $\tau_h \to \infty$ theory), and if the electron injection current density G and hole injection rate

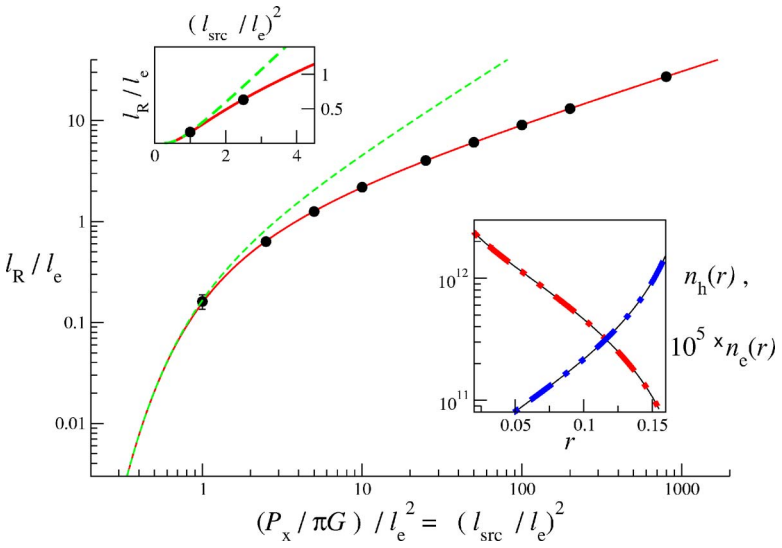

FIG. 3. (Color online) Radius, in units of l_e, plotted against P_x, in units of $\pi G l_e^2$. The dots are from numerical simulations, the solid line is the improved theory of Sec. III B, and the dashed line is the theory of Sec. III A. The upper inset displays the same curves in linear scale to give a sense of how the curves cross over from inverse-exponential to power-law behavior as l_{src} crosses l_e. In the lower inset: Negative-slope curve is $n_h(r<l_R)$, fitted (thick dashed line) with Eq. (10). Positive-slope curve is $n_e(r<l_R)$, magnified by *five orders of magnitude*, with the thick dashed line showing a fit by Eq. (11).

P_x are both changed while their ratio $P_x/G=\pi l_{src}^2$ is kept fixed (another prediction of the theory). In each of these cases the width of the interface is modified, as discussed in Sec. III D.

In Fig. 2(b), the steady-state hole density profile obtained from simulation of Eqs. (1) is compared to the logarithmic prediction, Eq. (3). The agreement is reasonable but imperfect; an improvement will be found in the next section.

In Fig. 2(c), the expression (4) for the electron densities outside the ring, $n_e(r>l_L)$, is tested against simulation data. There is some deviation at large distances, which remains unexplained. The density profiles of Figs. 2(b) and 2(c) are taken from a steady-state solution with $l_R \approx 0.18$.

Finally, in Fig. 2(d), the radius of the circular interface, obtained from direct simulation of Eq. (1), is plotted against hole injection intensities P_x. This is compared with Eq. (7), plotted as a solid line. The $l_R \ll l_e$ limit is shown by a dashed line. For larger radii ($l_R > l_e$ and $l_{src} > l_e$), the prediction for the radius is seriously at odds with the numerical results. The simulations suggest that the dependence on P_x/G follows a lower exponent than the linear dependence obtained in this section. This discrepancy is corrected in the next section.

B. Corrections from "dark" interior

We now turn our attention to the hole-rich region within the ring, at radial distances $r<l_R$, far enough from the reaction front so that $n_h \gg n_e$. We will now encounter effects of the extended source term for the electrons, i.e., of the position-independent G. Taking account of these effects turns out to be the key to overcoming the failure in Sec. III A to predict the ring radius for $l_R \gg l_e$.

Some of the figures published by Ref. [1,3] suggest a nonzero luminescence intensity in the nominally dark region between the inner spot and the ring. The small but nonzero intensity in the ring interior seems to be roughly constant between the inner spot and the ring, but a more quantitative statement is hard to extract from the published figures. To the best of the present author's knowledge, this feature has not been explained previously.

In numerical results (e.g., in Fig. 1 and also in Fig. 1c of Ref. [3]), one feature of the luminescence ($\gamma n_h n_e$) curve is that it is nonzero and very nearly constant in most of the supposedly dark interior of the ring. The constant value is found to be equal to G, the electron influx density. In other words, our reaction zone has an "extended" part in the hole side of the interface.

To explain the constant luminescence for $r<l_R$, as seen in the numeric simulations and possibly in the experiments, we relax the assumption that $n_e(r)$ vanishes completely inside the ring ($r<l_R$). In the steady-state equation for the electron density, Eq. (2b), the tunneling term can be neglected compared to G because $n_e(r<l_R) \ll n_e(\infty)=G\tau_e$. The diffusion term is also small because, away from the interface, n_e is small and smoothly varying. (This is justified more rigorously, *a posteriori*, in Appendix B.) We are left with $\gamma n_h(r) n_e(r) \approx G$, as required.

A finite $\gamma n_h n_e$ also affects the steady-state hole density distribution. Feeding $\gamma n_h n_e = G$ into Eq. (2a), we get a correction to the expression (3) for the hole density:

$$n_h(r<l_R) = \frac{P_x}{2\pi D_h}\ln\left(\frac{l_R'}{r}\right) + \frac{G}{4D_h}r^2 = \frac{P_x}{2\pi D_h}\left[\ln(l_R'/r) + \frac{r^2}{2l_{src}^2}\right], \tag{10}$$

with $l_R' \neq l_R$. Assuming the luminescence peak to be sharp enough, using the condition $n_h(r=l_R)=0$ yields $l_R' = l_R \times \exp[-l_R^2/2l_{src}^2]$.

The lower inset to Fig. 3 shows that Eq. (10), with the $(G/4D_h)r^2$ term included, provides perfect agreement with the numerical simulations. This can be compared to the previous attempt [Fig. 2(b)]. The same inset also shows the electron density in the hole region (much magnified), perfectly obeying

$$n_e(r<l_R) = \frac{G/\gamma}{n_h(r<l_R)} = \frac{2D_h/\gamma}{l_{src}^2\ln(l_R'/r) + 1/2r^2}. \tag{11}$$

Note that the decay of n_e as one moves away from the interface is not exponential or even power law, but much weaker.

The l_R' that gives the best fit to the n_h and n_e curves is also in excellent agreement with the prediction above.

An even more dramatic improvement occurs with the prediction for the radius, which we determine, as before, by imposing $D_h|n_h'(l_R)|=D_e|n_e'(l_R)|$:

$$\frac{1}{2l_R}(l_{src}^2 - l_R^2) = l_e \frac{K_1(l_R/l_e)}{K_0(l_R/l_e)}. \tag{12}$$

Figure 3 shows how the peak postions obtained from direct simulation of the diffusion-reaction Eqs. (1) are perfectly explained by Eq. (12). The discrepancy of our original attempt following Ref. [3], as shown in Fig. 2(a), has been solved.

The $l_R \gg l_e$ and $l_R \ll l_e$ limits are, respectively,

$$l_R = -l_e + \sqrt{l_e^2 + (P_x/\pi G)} = -l_e + \sqrt{l_e^2 + l_{src}^2}$$

and

$$l_R = l_e \exp\left[-\frac{2l_e^2}{l_{src}^2 - l_R^2}\right] \approx l_e \exp\left[-\frac{2l_e^2}{l_{src}^2}\right].$$

From the solution of Eq. (12), e.g., from Fig. 3, one observes that l_{src}/l_e also tends to be large for $l_R \gg l_e$. Using this additional information, the $l_R \gg l_e$ expression reduces to $l_R \approx l_{src} = \sqrt{P_x/\pi G}$. This explains the straight line in the log-log plot of Fig. 3 for large l_R/l_e. The line has a slope half of that in the case of the simple theory without an interior correction, Fig. 2(a), where the behavior is $l_R \propto P_x$. It is remarkable that the tiny $n_e(r<l_R)$, orders of magnitude smaller than $G\tau_e$ or $n_h(r<l_R)$, actually modifies the global structure of the steady-state configuration.

C. Finite hole tunneling

We now relax the approximation of infinite hole leakage time scale τ_h, so that the hole depletion length $l_h=\sqrt{D_h\tau_h}$ is finite and can play a role. Equation (3) for the hole density is now corrected to

$$n_h(r) = \frac{P_x}{2\pi D_h} K_0\left(\frac{r}{l_h}\right)\theta(l_R - r). \tag{13}$$

For $r \ll l_h$, the K_0 solution reduces to a logarithm, as before.

Note that, since the K_0 function does not vanish for finite arguments, the radius l_R cannot be built into $n_h(r<l_R)$ as a boundary condition. The discontinuity in Eq. (13) suggests that the structure of the interface plays a more important role here compared to the $l_h \to \infty$ case. In addition, Eq. (13) also allows us to infer the ring radius l_R using "physical" arguments. The discontinuity can be minimized by having $l_R > l_h$, because the $K_0(x)$ function crosses over to $\sim e^{-x}/\sqrt{x}$ for $x>1$. On the other hand, l_R cannot be too much larger than l_h, since the hole flux also decreases exponentially for $l_R > l_h$. The radius is therefore expected to be slightly larger than the hole depletion length l_h, for a range of parameters.

As in Sec. III B, one should correct for nonzero $\gamma n_h(r)n_e(r)$, at $r<l_R$

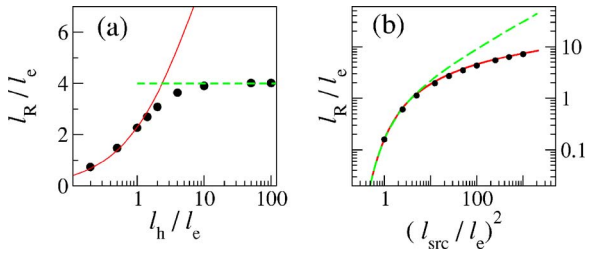

FIG. 4. (Color online) Ring radius with finite hole tunneling. (a) Variation with hole depletion length l_h, for $P_x=25\pi G$. (b) Variation with $P_x/\pi G$, for $l_h=\sqrt{2}l_e$. In each plot, dots are from direct simulation of Eqs. (1). Solid curves are the prediction of Eq. (16) and dashed curves are the $l_h=\infty$ result, Eq. (12).

$$n_h(r<l_R) = \frac{P_x}{2\pi D_h} K_0\left(\frac{r}{l_h}\right) - G\tau_h, \tag{14}$$

and

$$n_e(r<l_R) = \frac{2D_h/\gamma}{l_{src}^2 K_0(r/l_h) - 2l_h^2}. \tag{15}$$

Since the correction to $n_h(r)$ is a constant, the extended part of the reaction zone loses the crucial role it had for $l_h \to \infty$ in the determination of the interface position l_R. Assuming again an infinitely sharp interface at l_R and equating currents,

$$\frac{P_x}{2\pi l_h} K_1(l_R/l_h) = G l_e \frac{K_1(l_R/l_e)}{K_0(l_R/l_e)}. \tag{16}$$

In the $l_R \gg l_e$, $l_R \gg l_h$ limit,

$$l_R = \frac{1}{2} l_h W_0\left(\frac{P_x/4G}{l_e^2 l_h^2}\right) = \frac{1}{2} l_h W_0\left(\frac{\pi}{4}[l_{src}/\sqrt{l_e l_h}]^4\right). \tag{17}$$

Here $W_0(x)$ is the principal branch of the Lambert W function [23]. The large-l_R behavior for comparable l_h and l_e is thus logarithmlike rather than power law. Unsurprisingly, in the $l_R \ll l_e$, $l_R \ll l_h$ limit, one recovers the $l_R \ll l_e$ limit of Secs. III A and III B, $l_R = l_e \exp[-2l_e^2/l_{src}^2]$.

Figure 4(a) shows the dependence of the radius on the hole tunneling. At small l_h, the radius obeys Eq. (16) well. As predicted, here the radius tends to be somewhat larger than but of the order of the hole depletion length l_h. At large l_h, the ring radius approaches the $l_h=\infty$ result of Eq. (12). There is an intermediate range of l_h where neither equations work. For the case shown in Fig. 4(a), this crossover region is $2l_e \lesssim l_h \lesssim 10l_e$. Presumably, an analytic understanding of this parameter region requires taking into account the interface structure details. The author has not been able to incorporate effects of interface structure into the prediction for the radius.

Figure 4(b) shows for $l_h=\sqrt{2}l_e$ the radius as a function of the hole source intensity. For this l_h/l_e, Eq. (16) still works extremely well.

D. Width and structure of interface

The width l_w of steady-state reaction fronts in diffusion-limited reaction processes is known from heuristic arguments

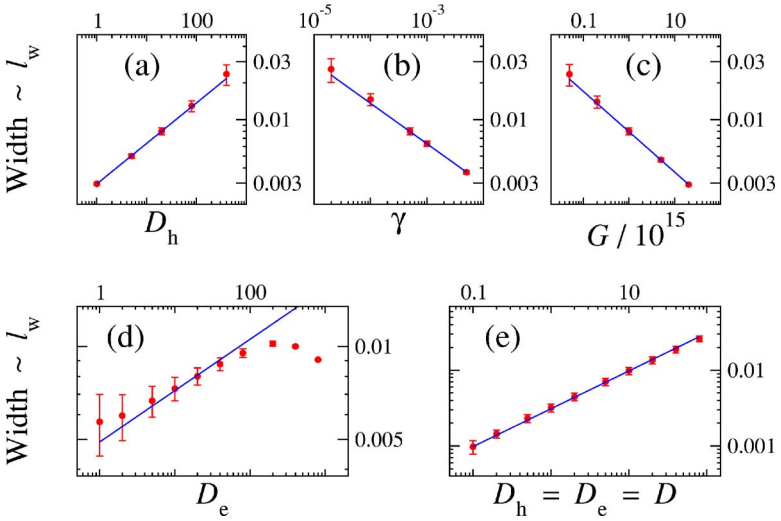

FIG. 5. (Color online) Width (full width at half maximum) of the luminescence peak, from steady states obtained by simulation, plotted (log-log) against various parameters. The error bars reflect the fact that one could choose half maximum using either G or zero as the base value of the luminescence $\gamma n_e n_h$, since $\gamma n_e n_h$ falls to G on one side of the peak and to zero on the other side. In (c), G is varied while keeping the ratio $P_x/G = \pi l_{src}^2$ constant. In (e), D_h and D_e are varied together. The straight lines are power-law fits with exponents (a) $\frac{1}{3}$ for D_h, (b) $-\frac{1}{3}$ for γ, (c) $-\frac{1}{3}$ for G, (d) $\frac{1}{6}$ for D_e, and (d) $\frac{1}{2}$ for $D=D_h=D_e$.

[7,12] to scale as $(D_h D_e/\gamma J)^{1/3}$, where J is the flux of particles entering the interface region.

In Fig. 5 the steady-state interface width, obtained by simulation of Eqs. (1), is displayed as a function of various parameters. While the variations with the hole diffusion D_h and the annihilation rate γ do follow $\pm\frac{1}{3}$ exponents quite closely, the dependence on the electron diffusion D_e is much weaker. To understand this, one has to consider the particle flux J. For both cases of infinite and finite τ_h, the flux of electrons into the interface region is $J = G l_e [K_1(l_R/l_e)/K_0(l_R/l_e)]$. There is complicated dependences on the ring position l_R, but in the $l_R \gg l_e$ limit one can use $[K_1(x)/K_0(x)] \overset{x\gg 1}{\longrightarrow} 1$ to simplify

$$l_w \sim \left(\frac{D_h D_e}{\gamma G l_e}\right)^{1/3} = \frac{D_h^{1/3} D_e^{1/6}}{\gamma^{1/3} G^{1/3} \tau_e^{1/6}}. \tag{18}$$

The variation of the numerically determined width with G [Fig. 5(c)] is also in accord with this prediction. In Figs. 5(a)–5(c) the ring position l_R is unchanged.

The variation with D_e shown in Fig. 5(d) is more complex; in this case l_R also changes with D_e. While the exponent $\frac{1}{6}$ works reasonably for an intermediate range of D_e, there is a significant deviation at larger D_e because the ring radius l_R gets smaller, leading to a breakdown of the $K_1/K_0 \approx 1$ approximation. At small D_e, the interface width is difficult to define because the interface becomes highly asymmetric for $D_e \ll D_h$, as indicated by the large error bars in Fig. 5(d). In Fig. 5(e) both diffusion constants are varied together. The interface width is now better defined over a wide range and the exponent $\frac{1}{2}$ (from $D_h^{1/3} D_e^{1/6} = D^{1/3+1/6} = D^{1/2}$) works very well.

The detailed structures of $n_{h,e}$ at the interface are difficult to put in closed form. Within this region $n_e(r)$ crosses over from its $r < l_R$ behavior, Eq. (11) or (15), to its $r > l_R$ solution, Eq. (2b). In the same region, the hole density crosses over from its interior solution, Eq. (10) or (14), to its $r > l_R$ solution which we have not considered yet. For $r > l_R + l_e$, where n_e has reached $n_e(r=\infty) = G\tau_e$, the hole density decays fast, as $K_0(r/l_{out})$, with the small decay length $l_{out} = \sqrt{D_h/G\tau_e\gamma} = l_w\sqrt{l_w/l_e}$.

We will not attempt to extract details of the crossover, which can, in principle, be obtained with a l_w/l_R expansion, similar to boundary-layer theory [24] developed in the context of fluid flows near boundaries.

IV. DISCUSSION

Although motivated by particular solid-state experiments, it is instructive to consider this analysis in the context of theoretical investigations of steady-state diffusion-limited reaction fronts and closely related situations. A thorough study of a simple steady-state front, with diffusion and annihilation terms and equal and opposite currents, appears in Ref. [7]. Our calculations are in the same spirit, but we have specific source and decay terms in addition, which play crucial roles. A related (and more often studied) phenomenon is that of time-dependent fronts, where two species are initially well-segregated [9–11]. Many of the same considerations apply, with powers of inverse time ($t^{-\alpha}$) playing a similar role as the particle flux J does in the steady-state case. Geometries similar to ours have been considered in Refs. [14,15,25], where one species of the reaction-annihilation pair forms an island in a sea of the other.

We have limited ourselves to the mean-field diffusion-reaction equations (1). In principle, mean-field treatments are valid only above the critical dimension, which happens to be 2. At and below the critical dimension, fluctuations become important [8,10–13]. In the 2D system of the present paper, effects of fluctuations may show up in several ways. First, the form of the annihilation term we have used, $\gamma n_h n_e$, can be expected to have logarithmic corrections in 2D [8]. Logarithmic corrections are also expected for the power-law scaling of the width [8,11,12]. We justify the mean-field approximation by noting that almost all the quantities we have considered involve large numbers of particles so that fluctuations are unimportant.

We have assumed that the charged carriers annihilate directly, neglecting the diffusion, dissociation, and quantum dynamics of bound excitons [19,20]. Exciton diffusion might

cause the observed luminescence width to be larger than what corresponds to $\gamma n_h n_e$ in our model, but the overall trends of Sec. III D are not expected to be affected severely. We have also ignored possible effects of quantum degeneracy of the charged carriers, which could change the form of the diffusion terms, so that $D_{h,e}$ are themselves density-dependent [5]. All effects of Coulomb interactions, including screening effects from the conducting leads [5,6,20], have also been left out of our formulation, because the treatment of Coulomb and screening effects would require detailed modeling more appropriate for a separate study.

In their brief analytic treatment of the steady state, Butov *et al.* [3] have assumed $l_h=\infty$ (lack of hole tunneling decay) and $l_R \ll l_e$. Our results of Sec. III C allow an assessment of the $l_h=\infty$ approximation (Secs. III A and III B, and Ref. [3]). Figure 4(a) shows that it is reasonable for $l_h \gtrsim 10 l_e$, but breaks down for smaller l_h. Since $\tau_h > \tau_e$ is typical in the experimental realizations, the $l_h=\infty$ results may well be experimentally relevant in some cases.

On the other hand, the $l_R \ll l_e$ approximation is more questionable. First, with the $l_R \sim \exp[-\lambda/P_x]$ behavior, a relatively small change in P_x can induce an orders-of-magnitude change in l_R. This implies that fluctuations in the effective P_x would cause the ring position to fluctuate wildly, so that the stable luminescence ring pattern would be unlikely to have been observed. (Such fluctuations have also been observed in the numerical simulations for $l_R \lesssim l_e$.) Second, experimental data on the ring radius as a function of laser power [5,6] show power-law behavior rather than any strong $\exp[-\lambda/P_x]$-like behavior. While the relationship between P_x and the power is not known, it is unlikely to compensate for the $\exp[-\lambda/P_x]$ behavior and give power-law-like l_R-vs-power curves. It is, therefore, important to consider the $l_R \gg l_e$ case in detail, as we have done.

We now comment on the experimental l_R vs laser power data [5,6]. The nonmonotonic behavior in Fig. 5 of Ref. [6] strongly indicates that the dependence of the P_x parameter of our model on the laser power is complicated. Note that P_x is an effective parameter measuring the amount of *excess* holes diffusing out of the laser irradiation region. To the best of the author's knowledge, the process of generating excess holes has not been modeled quantitatively, and nothing is known conclusively about the P_x-power dependence. Equations (12) and (16), which express the radius l_R in terms of P_x, cannot be used to fit the experimental l_R vs laser power data without additional assumptions about the P_x-power relationship.

In Ref. [5], Denev *et al.* have suggested that the linear behavior of l_R vs power might be due to the importance of Coulomb terms which are not included in the present diffusion-reaction model. However, if the effective P_x parameter increases quadratically with the laser power, our $l_R \propto \sqrt{P_x}$ prediction for $l_h \gg l_e$ would also show up as a linear l_R-power result.

Our analytic results gives insight into other simulations, for example, the numerical results in Fig. 1b of Ref. [5]. The fact that this curve behaves roughly logarithmically at large l_R (large P_x), rather than as a power law with exponent $\frac{1}{2}$, shows that the simulations were done using finite τ_h, with l_h not too large compared to l_e. Note that the Lambert W function of Eq. (17) is roughly logarithmic for large arguments, $W_0(x \to \infty) \approx \log_{10} x - \log_{10}(\log_{10} x)$.

The width of the reaction front is expected to be even more difficult to study experimentally than the radius. Experimental study of the width requires finer spatial resolution, and the parameters involved in Eq. (18) are difficult to tune individually. The steady-state density distributions Eqs. (10), (11), (14), and (15) are also not easily measurable in the electron-hole experimental system that motivates our study. An alternative realization, using, for example, osmosis from a reservoir to mimic the electron source term G and osmosis into a 2D sink to mimic the tunneling decays, would be useful for studying effects analyzed here.

To summarize, motivated by semiconductor luminescence experiments, we have investigated a two-species inhomogeneous steady state arising from mean-field diffusion-annihilation equations with a localized source for one species and an extended source for the other. The source asymmetry results in a luminescence profile that is a *nonzero constant* on the hole side of the interface; this feature is also visible in some of the experimental pictures. If the holes are not allowed to have single-particle (tunneling) decay, our analytic solutions for the density profiles and the radius of the ring-shaped interface are spectacularly successful, as seen from comparisons to simulation data. When both species are allowed to tunnel out, the quality of the analytic predictions is more modest. We have detailed the crossover between finite hole tunneling and zero hole tunneling behaviors of the interface position. The thorough study of the steady state presented here should serve as a baseline for evaluating the need to invoke additional physical effects for explaining experimental observations.

ACKNOWLEDGMENTS

The author thank G. Barkema, C.J. Fennie, P.B. Littlewood, D. Panja, S. Pankov, I. Paul, L. Pfeiffer, P. M. Platzman, M. W. J. Romans, W. van Saarloos, and D. Snoke for discussions, and H.T.C. Stoof for his generosity and mentorship. Funding was provided by the Nederlandse Organisatie voor Wetenschaplijk Onderzoek (NWO).

APPENDIX A: NUMERICAL SIMULATIONS

The numeric steady states have been obtained by following in time the evolution of Eqs. (1). The one-dimensional spatial grid was not linear but chosen to be concentrated at smaller radial distances. The time evolution due to the diffusion terms was performed by a symmetric combination of forward and backward Euler evolution. This is sometimes called the "improved Euler method" and has error $O(\delta t^3)$ per time step. The time steps δt themselves were determined adaptively, and kept small enough such that the diffusion terms would not decrease densities below zero.

The terms other than diffusion were treated "exactly" within each time step, i.e., to order $O(\delta t^\infty)$. For holes, the change $n_h(t+\delta t) - n_h(t)$ is given by

$$\delta n_h = [n_h(t) - P_h e^{-r^2/lL^2}/\lambda_e][e^{-\lambda_e \delta t} - 1],$$

where $\lambda_e = \gamma n_e(t) + 1/\tau_e$ acts as a decay factor. The electron evolution in each time step is similar with the source G instead of $P_h e^{-r^2/lL^2}$.

APPENDIX B: SMALL ELECTRON DIFFUSION IN INTERIOR, JUSTIFIED

To justify the neglect in Sec. III B of the diffusion term $D_e \nabla^2 n_e$ compared to G in the $r < l_R$ region, one can use $n_e(r) \approx G/\gamma n_h(r) \approx 2D_h[l_{src}^2 \gamma \ln(l_R/r)]^{-1}$ to estimate the diffusion term. The result can be expressed as

$$\frac{|D_e \nabla^2 n_e|}{G} \sim l_w^3 \frac{l_e}{l_{src}^2 l_R^2} = \left(\frac{l_w}{l_R}\right)^3 \frac{l_R/l_e}{(l_{src}/l_e)^2}.$$

Using the observation $(l_{src}/l_e)^2 > (l_R/l_e)$, from Fig. 3 or Fig. 4, we see that a sufficient condition for $D_e \nabla^2 n_e/G$ to be negligible is $l_w \ll l_R$, which is true as long as there is a well-defined interface.

[1] L. V. Butov, A. C. Gossard, and D. S. Chemla, Nature (London) **418**, 751 (2002).
[2] D. Snoke, S. Denev, Y. Liu, L. Pfeiffer, and K. West, Nature (London) **418**, 754 (2002).
[3] L. V. Butov, L. S. Levitov, A. V. Mintsev, B. D. Simons, A. C. Gossard, and D. S. Chemla, Phys. Rev. Lett. **92**, 117404 (2004).
[4] R. Rapaport, G. Chen, D. Snoke, S. H. Simon, L. Pfeiffer, K. West, Y. Liu, and S. Denev, Phys. Rev. Lett. **92**, 117405 (2004).
[5] S. Denev, S. Simon, and D. Snoke, Solid State Commun. **134**, 59 (2005).
[6] D. Snoke *et al.*, e-print cond-mat/0406141.
[7] E. Ben-Naim and S. Redner, J. Phys. A **25**, L575 (1992).
[8] P. L. Krapivsky, Phys. Rev. E **51**, 4774 (1995).
[9] L. Gálfi and Z. Rácz, Phys. Rev. A **38**, 3151 (1988).
[10] B. P. Lee and J. Cardy, Phys. Rev. E **50**, R3287 (1994).
[11] S. Cornell, M. Droz, and B. Chopard, Phys. Rev. A **44**, 4826 (1991).
[12] S. Cornell and M. Droz, Phys. Rev. Lett. **70**, 3824 (1993).
[13] G. T. Barkema, M. J. Howard, and J. L. Cardy, Phys. Rev. E **53**, R2017 (1996).
[14] B. M. Shipilevsky, Phys. Rev. E **67**, 060101(R) (2003).
[15] B. M. Shipilevsky, Phys. Rev. E **70**, 032102 (2004).
[16] M. C. Cross and P. C. Hohenberg, Rev. Mod. Phys. **65**, 851 (1993).
[17] A. J. Koch and H. Meinhardt, Rev. Mod. Phys. **66**, 1481 (1994).
[18] J. P. Gollub and J. S. Langer, Rev. Mod. Phys. **71**, S396 (1999).
[19] L. S. Levitov, B. D. Simons, and L. V. Butov, Phys. Rev. Lett. **94**, 176404 (2005).
[20] L. S. Levitov, B. D. Simons, and L. V. Butov, Solid State Commun. **134**, 51 (2005).
[21] G. Chen, R. Rapaport, S. H. Simon, L. Pfeiffer, and K. West, Phys. Rev. B **71**, 041301(R) (2005).
[22] L V Butov, J. Phys.: Condens. Matter **16**, R1577 (2004).
[23] R. M. Corless, G. H. Gonnet, D. E. G. Hare, D. J. Jeffrey, and D. E. Knuth, Adv. Comput. Math. **5**, 329 (1996); R. M. Corless, D. J. Jeffrey, and D. E. Knuth, Proceedings of the ISSAC '97, edited W. Kuechlin (ACM Press, New York, 1997); J.-M. Caillol, J. Phys. A **36**, 10431 (2003).
[24] For an example of using boundary-layer methods for correcting approximate solutions with kinks, see F. Dalfovo, L. Pitaevskii, and S. Stringari, Phys. Rev. A **54**, 4213 (1996); A. L. Fetter and D. L. Feder, *ibid.* **58**, 3185 (1998); where the authors calculate corrections to the Thomas-Fermi density profiles of trapped Bose-Einstein condensates.
[25] H. Larralde, Y. Lerean, P. Trunfio, J. Dror, S. Havlin, R. Rosenbaum, and H. E. Stanley, Phys. Rev. Lett. **70**, 1461 (1993); A. D. Sánchez, S. Bouzat, and H. S. Wio, Phys. Rev. E **60**, 2677 (1999); W. Hwang and S. Redner, *ibid.* **64**, 041606 (2001).